



## Subgrid modeling of moveable-bed bottom friction in wind wave models<sup>1</sup>

Hendrik L. Tolman

UCAR visiting scientist, Ocean Modeling Branch, Environmental Modeling Center, NOAA/NCEP,  
5200 Auth Road, Room 209, Camp Springs, MD 20746, USA

Received 23 December 1994; accepted 22 May 1995

### Abstract

A subgrid moveable-bed bottom friction model is developed for use in large-scale wind wave models. This model defines a representative bottom roughness based on the local application of a discontinuous roughness model and a statistical description of depth, sediment and wave parameters for a finite area within the model (i.e., a grid box). The model reproduces the discontinuous attenuation behavior of swell in conditions of initial ripple formation as predicted by a small-scale model. It furthermore suppresses non-physical oscillations of swell energy and unrealistically strong dependencies of depth-limited wave heights on sediment parameters. An alternative interpretation of the model explains the (continuous) transition between the no-ripple and ripple regimes as sometimes observed in nature.

### 1. Introduction

In the modeling of wind-waves in shallow water, bottom-friction plays an important role (e.g., Shemdin et al., 1978; SWIM Group, 1985). The hydrodynamics of bottom friction for wind waves are fairly well understood (e.g., Weber, 1991). Modeling bottom friction, however, is complicated by interactions between waves and sediment. Wave-sediment interactions manifest as ripple formation and as apparent roughness related to sheet flow of sediment in the wave boundary layer. Ripple formation can have a dramatic effect on the bottom roughness length scale  $k_N$  (Nikuradse equivalent sand grain roughness); the roughness can range from skin friction with  $k_N = O(10^{-4} \text{ m})$ , to well developed ripples with  $k_N = O(10^{-1} \text{ m})$ . This large range of possible roughnesses qualitatively explains the large range of decay scales and friction factors observed for swell (Shemdin et al., 1978). A moveable-bed roughness model has been available for over a decade (Grant and Madsen,

<sup>1</sup> OPC contribution Nr. 102.

1982). Although this model appears to be well established in the sediment transport community, it has been implemented (to the knowledge of the present author) in a wave model only once (Graber and Madsen, 1988).

Recently, Tolman (1994) assessed the potential effects of moveable-bed roughness for wind waves using a modified version of the Grant and Madsen roughness model. By analyzing spatial decay scales of the wave field, Tolman has shown that moveable-bed roughness and initial ripple formation are potentially important for swell propagation in shelf seas away from the shore [that is, where horizontal scales of the bathymetry are  $O(10 \text{ km})$  or larger]. In such conditions, the roughness is governed by the decay rate of the wave field, as will be illustrated in section 2. Moveable-bed effects are not expected to dominate severely depth-limited wind seas, because such wave conditions usually result in vigorous near-bottom wave motion. Bed forms then are washed out and roughnesses are generally small and exhibit limited variability.

Tolman (1994) advocates a subgrid approach when a moveable-bed roughness model is implemented in a large-scale wave model because (i) the spatial decay scales for swell in conditions of initial ripple formation are generally not resolved by wave models, and because (ii) a single roughness might not be representative for an entire grid box in conditions of initial ripple formation. Note that subgrid modeling is not expected to be relevant for severely depth-limited wind seas, as the corresponding roughness regimes are generally far removed from the discontinuity of the roughness model. However, initial ripple formation does result in large changes of the roughness for mildly depth-limited wind seas, where subgrid modeling might influence model behavior.

The present paper addresses subgrid modeling of moveable-bed bottom friction. The starting point is the hydrodynamic model of Madsen et al. (1988) and a modified version of the roughness model of Grant and Madsen (1982) as used by Tolman (1994) (see section 2). This model is shown to result in quasi-random behavior in space, if the required depth and sediment parameters are described with minimal random variability. In section 3 and in the Appendix a statistical subgrid model is derived. In section 4 this model is applied successfully to an idealized swell case and to an idealized case of depth-limited wave growth. The latter case indicates that a subgrid approach is necessary to avoid nonphysical behavior of a wave model for mildly depth-limited wind seas. In section 5 the application of the present subgrid approach to other moveable-bed roughness parameterizations, and the smooth transition between the no-ripple and ripple regimes as observed by Amos et al. (1988) are discussed.

## 2. Moveable-bed bottom friction

The (local) bottom-friction source term used in the present study consists of the hydrodynamic model of Madsen et al. (1988) and a modified version of the roughness model of Grant and Madsen (1982) as defined by Tolman (1994).

The hydrodynamic model relates a bottom-friction source term  $S_b$  to the corresponding two-dimensional spectrum  $F$ . This spectrum can be either the wavenumber spectrum  $F(k)$ , the wavenumber-direction spectrum  $F(k, \theta)$ , or the frequency-direction spectrum  $F(f, \theta)$ .

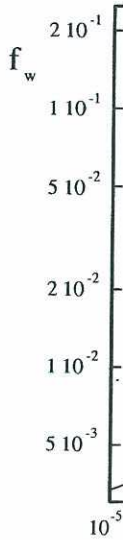


Fig. 1. The friction factor function of the relative

$$S_b = -f_w u_r \frac{\bar{c}}{2g}$$

$$f_w = \frac{1}{K e r^2 (2\sqrt{c})}$$

$$s_0 = \frac{1}{21.2 \kappa \sqrt{f_w}}$$

$$u_r = \left( \frac{2\omega^2}{\sinh^2 kd} \right)^{1/2}$$

where  $\omega = 2\pi f$  is the angular frequency,  $K$  is the Nikuradse roughness function of the zero roughness  $k_N/a_r$  or representative near wave sediment number  $\psi$

$$\psi = \frac{f_w' u_r^2}{2(s-1)g}$$

where  $s$  is the relative roughness  $D$  is a representative

in the sediment transport component (author) in a wave model

of moveable-bed roughness for Madsen roughness model. By has shown that moveable-bed important for swell propagation in les of the bathymetry are  $O(10$  d by the decay rate of the waves ts are not expected to dominate tions usually result in vigorous and roughnesses are generally

veable-bed roughness model is atial decay scales for swell in d by wave models, and because ntire grid box in conditions of ected to be relevant for severely imes are generally far removed tial ripple formation does result ind seas, where subgrid mod-

able-bed bottom friction. The (1988) and a modified version used by Tolman (1994) (see havior in space, if the required ndom variability. In section 3 section 4 this model is applied d case of depth-limited wave necessary to avoid nonphysical as. In section 5 the application ghness parameterizations, and es as observed by Amos et al.

nt study consists of the hydro- sion of the roughness model of

e term  $S_b$  to the corresponding e wavenumber spectrum  $F(k)$ , y-direction spectrum  $F(f, \theta)$ .

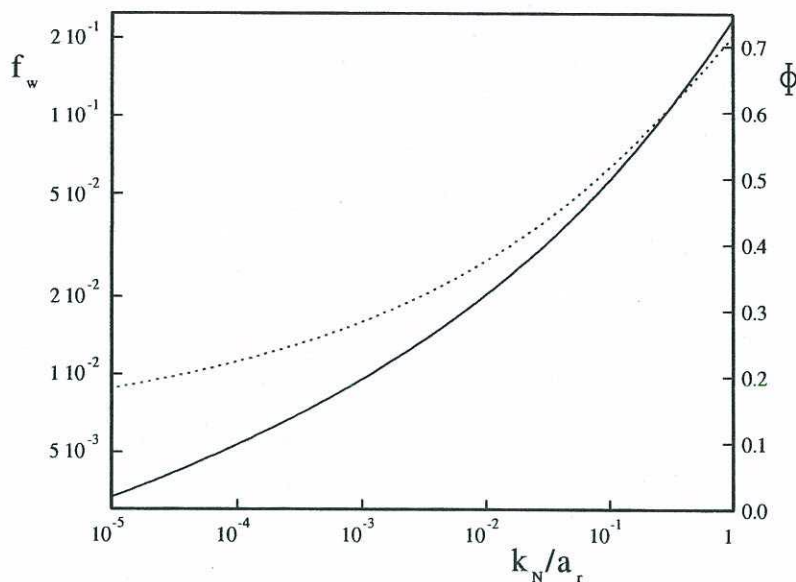


Fig. 1. The friction factor  $f_w$  (Eqs. 2 and 3, solid line) and its normalized derivative  $\Phi$  (Eq. 17, dotted line) as a function of the relative roughness  $k_N/a_r$ .

$$S_b = -f_w u_r \frac{\omega^2}{2g \sinh^2 kd} F \quad (1)$$

$$f_w = \frac{0.08}{Ker^2(2\sqrt{s_0}) + Kei^2(2\sqrt{s_0})} \quad (2)$$

$$s_0 = \frac{1}{21.2\kappa\sqrt{f_w}} \frac{k_N}{a_r} \quad (3)$$

$$u_r = \left( \frac{2\omega^2}{\sinh^2 kd} F \right)^{1/2}, \quad a_r = \left( \frac{2}{\sinh^2 kd} F \right)^{1/2} \quad (4)$$

where  $\omega = 2\pi f$  is the radian frequency,  $d$  is the depth,  $f_w$  is the wave friction factor,  $k_N$  is the Nikuradse roughness length,  $\kappa$  is the Von Kàrmàn constant and  $Ker$  and  $Kei$  are Kelvin functions of the zeroth order. The friction factor  $f_w$  (Fig. 1) is a function of the relative roughness  $k_N/a_r$  only and  $f_w$  is constant for  $k_N/a_r > 1$  ( $f_w = 0.236$ ). Finally,  $u_r$  and  $a_r$  are a representative near-bottom orbital velocity and amplitude, respectively.

Wave-sediment interaction occurs if the near-bottom wave motion is sufficiently strong to move sediment. The ability of the waves to move sediment is governed by the Shields number  $\psi$

$$\psi = \frac{f_w' u_r^2}{2(s-1)gD} \quad (5)$$

where  $s$  is the relative density of the sediment compared to water (2.65 for quartz sands),  $D$  is a representative grain diameter and the prime in  $f_w'$  indicates that the friction factor is

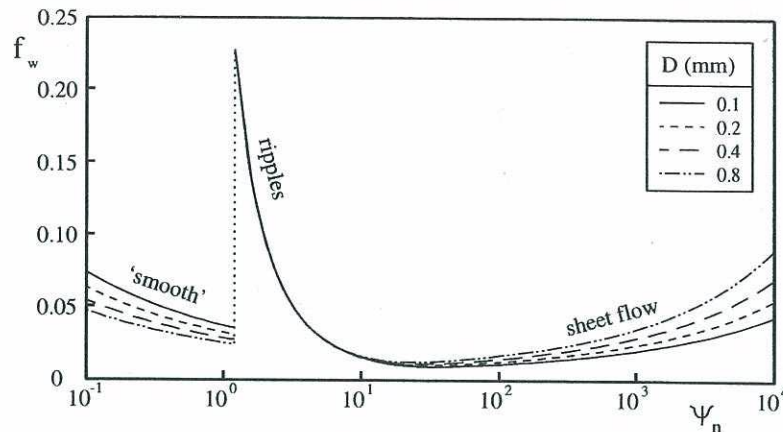


Fig. 2. The friction factor  $f_w$  as a function of the normalized Shields number  $\psi_n = \psi/\psi_c$  for the moveable-bed roughness model (Eqs. 6, 2 and 3) for various grain diameters  $D$ ,  $\psi_c = 0.05$ ,  $k_{N,0} = 0.01$  m and swell with  $f = 0.1$  Hz.

based on skin friction (that is, using  $k_N = D$  in Eq. 3). Sediment motion occurs if the Shields number becomes larger than its critical value for initial motion  $\psi_c$  (usually determined for monochromatic waves). The critical Shields number ranges from 0.04 to 0.06 for clean, well-sorted sands, to 0.20 or larger for bioturbated or multimodal sands (e.g., Madsen and Grant, 1976; Glenn and Grant, 1987; Drake and Cacchione, 1986; Cacchione et al., 1987; Gross et al., 1992).

If the wave motion is too weak to cause sediment motion (defined here as  $\psi/\psi_c < 1.2$ ), the roughness is set to a pre-defined base roughness  $k_{N,0}$ , which represents bioturbation, current-induced roughnesses and relict ripples. This roughness is typically of the order of 0.01 m or smaller (Tolman, 1994). If the wave motion is sufficiently strong to generate sediment motion ( $\psi/\psi_c \geq 1.2$ ), the relative roughness  $k_N/a_r$  becomes

$$\frac{k_N}{a_r} = 1.5 \left( \frac{\psi}{\psi_c} \right)^{-2.5} + 0.0655 \left( \frac{u_r^2}{(s-1)ga_r} \right)^{1.4} \quad (6)$$

This equation represents a modified version of the model of Grant and Madsen (1982). The first term on the right represents ripple roughness, and is based on observations of Madsen and Rosengaus (1988) and Madsen et al. (1990). The second term represents sheet-flow roughness, and is based on the model of Wilson (1989). Note that this roughness model differs significantly from the original Grant and Madsen model (see Tolman, 1994, Fig. 2), and that this model is representative for irregular waves and therefore cannot be expected to describe observations for regular waves accurately (see Tolman, 1994, section 3). Furthermore, the model is based on limited laboratory data and requires additional verification. Finally, currents are disregarded in the model, and for simplicity will also be disregarded throughout this paper.

For a given wave frequency  $f$ , the relative roughness (Eq. 6) and hence the friction factor becomes a function of the normalized Shields number  $\psi_n \equiv \psi/\psi_c$  only (Fig. 2). If no sediment motion occurs ( $\psi_n < 1.2$ ) the bed is relatively smooth with fairly small friction factors [ $f_w = O(0.05)$ ]. In conditions of initial ripple formation ( $\psi_n = 1.2$ ) the roughness

discontinuously increases. As the normalized Shields number increases, the roughness increases moderately due to the increase in the bed's roughness  $k_{N,0}$  and the apparent roughness  $k_N$  (see Eq. 6). The apparent roughness  $k_N$  increases discontinuously in the ripple regime in Fig. 2 is shown.

The discontinuous behavior of the roughness model is much smaller than assumed). Even then, the roughness is much smaller, particularly when the spatial bathymetric scales (Tolman, 1994) are much smaller than the swell propagation, for

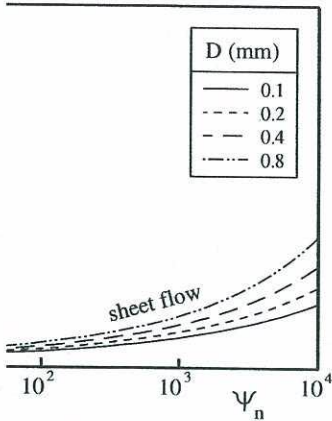
$$\frac{\partial c_g E}{\partial x} = S_t = -\frac{1}{4g} f_w^2$$

where  $E (= \int F)$  is the source term integrated over the depth. The equation are calculated (1994, Appendix), with a discontinuous range at A2 through A4).

Fig. 3 shows results for conditions chosen here. The roughness  $k_N$  is chosen to be 0.01 mm,  $\psi_c = 0.05 k_{N,0} = 0.0005$  m.

The solid lines in Fig. 3 describe the shoal water roughness model). The friction factor is nearly constant and corresponds to ripple formation (3c). Full ripple formation is reached at the maximum value of the roughness. This implies that the roughness is the dominant bathymetric scale.

The dotted lines in Fig. 3 show random variability added to the correlation at the grid scale. The grain diameter  $D$  and the added variability of the roughness model (3b) and Shields number resolution. The local roughness model as given in Fig. 3 results for the smooth bathymetric spatial decay scale correlation, and therefore is



Shields number  $\psi_n = \psi / \psi_c$  for the moveable-bed  $D, \psi_c = 0.05, k_{N,0} = 0.01$  m and swell with  $f = 0.1$

discontinuously increases to  $k_N/a_r \approx 1$  with  $f_w \approx 0.23$  (dotted line). For increasing Shields numbers ripples are washed out, resulting in a decrease of  $f_w$ . For  $\psi > 10^2$  friction factors increase moderately due to an increasing sheet-flow roughness. Note that both the “smooth bed” roughness  $k_{N,0}$  and the sheet flow roughness are independent of the grain diameter  $D$  (see Eq. 6). The apparent dependency the friction factor on  $D$  for the corresponding flow regimes in Fig. 2 is solely due to the dependency of  $\psi$  on  $D$  (Eq. 5).

The discontinuous behavior of the roughness model is realistic if the time scale of ripple generation is much smaller than the time scale of evolution of the wave field (as is generally assumed). Even then, the roughness can take any value in the discontinuous range, in particular when the spatial decay scale of the wave field is comparable to the dominant bathymetric scales (Tolman, 1994). This is illustrated below for steady, one-dimensional swell propagation, for which the governing equation is

$$\frac{\partial c_g E}{\partial x} = S_t = -\frac{1}{4g} f_w u_r^3 \tag{7}$$

where  $E$  ( $= \iint F$ ) is the total energy,  $c_g$  is the group velocity and  $S_t$  is the bottom friction source term integrated over the spectrum (from Eqs. 1 and 4). “Exact” solutions for this equation are calculated using the one-dimensional swell propagation model of Tolman (1994, Appendix), with a spatial resolution of 1 km. In this model, roughnesses within the discontinuous range are calculated from the overall energy balance (Tolman, 1994, Eqs. A2 through A4).

Fig. 3 shows results for a large-scale shoal (chain line in panel a). Sediment and wave conditions are chosen to assure ripple formation on the forward face of the shoal ( $D = 0.2$  mm,  $\psi_c = 0.05, k_{N,0} = 0.01$  m,  $T = 12$  s and, at the input boundary,  $H = 4\sqrt{E} = 1.75$  m).

The solid lines in Fig. 3 represent results for a bottom with a “smooth” bathymetry, describing the shoal with minimum variability (but obviously still allowing for ripples in the roughness model). In areas where no ripple formation occurs ( $\psi_n < 1.2$  in Fig. 3c), the friction factor is nearly constant and approximately 0.03 (Fig. 3b). Larger friction factors correspond to ripple roughness in conditions of initial ripple formation ( $\psi_n = 1.2$  in Fig. 3c). Full ripple formation does not occur as  $\psi_n$  does not exceed 1.2 and as  $f_w$  does not reach the maximum value corresponding to full ripple formation ( $f_w < 0.23$ , see Fig. 2). This implies that the spatial decay scale related to full ripple development is smaller than the dominant bathymetric scale.

The dotted lines in Fig. 3 represent results for a bathymetry and sediment data with random variability added. This variability has a normal distribution, and has no spatial correlation at the grid scale of the “exact” model (1 km). The standard deviation of the grain diameter  $D$  and critical Shields number  $\psi_c$  are  $\sigma_D = \sigma_{\psi_c} = 5\%$ , respectively, and the added variability of the depth  $\sigma_{d,random} = 0.25$  m. The corresponding friction factor (Fig. 3b) and Shields number (Fig. 3c) show quasi-random behavior on the scale of the model resolution. The local roughness no longer remains within the discontinuous range of the roughness model as generally  $\psi_n \neq 1.2$  (Fig. 3c). The wave height (Fig. 3a) follows the results for the smooth bathymetry (solid line) closely. This was expected, because the spatial decay scale corresponding to ripple formation is similar to the dominant bathymetric scales, and therefore much larger than the spatial scale of the added variability.

Sediment motion occurs if the Shields number  $\psi$  (usually determined for clean, fine-grained sands) ranges from 0.04 to 0.06 for clean, unimodal sands (e.g., Madsen and Cacchione, 1986; Cacchione et al., 1987;

sediment motion (defined here as  $\psi / \psi_c < 1.2$ ), the roughness  $k_{N,0}$ , which represents bioturbation, and the sheet flow roughness is typically of the order of magnitude of the sheet flow roughness. If the roughness is sufficiently strong to generate sheet flow,  $k_N/a_r$  becomes

$$(6)$$

The roughness model of Grant and Madsen (1982) is based on observations of sediment motion (Grant, 1990). The second term represents the roughness due to sediment motion (Wilson, 1989). Note that this roughness model is based on the Grant and Madsen model (see Tolman, 1994, section 2.2). For regular waves and therefore cannot be used for irregular waves accurately (see Tolman, 1994, section 2.2). Laboratory data and requires additional validation, and for simplicity will also be

used (Eq. 6) and hence the friction factor is a function of the Shields number  $\psi_n \equiv \psi / \psi_c$  only (Fig. 2). If no ripple formation occurs (smooth bed) the roughness is independent of the grain diameter (see Eq. 6). The apparent dependency the friction factor on  $D$  for the corresponding flow regimes in Fig. 2 is solely due to the dependency of  $\psi$  on  $D$  (Eq. 5).

$$\mathbf{X} = \begin{pmatrix} X_d \\ X_D \\ X_{\psi_c} \\ X_H \\ X_T \end{pmatrix} = \begin{pmatrix} \mathcal{F}(2 - \Phi') \\ -1 + \Phi' \\ -1 \\ 2 - \Phi' \\ [2\mathcal{F}(2 - \Phi')] - 2 \end{pmatrix} \quad (15)$$

where

$$\mathcal{F} = \frac{k_p d}{2n_p \tanh k_p d} \quad (16)$$

$$\Phi' = \frac{k_N/a_r}{f_w} \frac{\partial f_w}{\partial (k_N/a_r)} \quad (17)$$

$$n = \frac{k}{\sigma} \frac{\partial \sigma}{\partial k} = \frac{1}{2} + \frac{kd}{\sinh 2kd} \quad (18)$$

The prime in  $\Phi'$  indicates skin friction ( $k_N = D$ ) as in Eq. (5).

The factors  $\mathbf{X}$  represent amplification factors between the relative variance of components of  $\mathbf{x}$  (i.e.,  $\sigma_i/x_{i,m}$ ) and the relative spread of the normalized Shields number ( $\sigma_\psi/\psi_{n,m}$ ). Negative values indicate that an increase of  $x_i$  corresponds to a decrease of  $\psi_n$ .

The factors  $\mathbf{X}$  are a function of the relative depth  $k_p d$  and the normalized derivative of the friction factor for skin friction  $\Phi'$ . Water depths are generally considered depth-limited for  $k_p d < 3$ . A representative range of  $\Phi'$  can be estimated from Fig. 1. For sediment motion to occur,  $a_r$  is typically  $O(0.1 \text{ m})$  or larger. With  $k_N = D$   $O(1 \text{ mm})$  or smaller,  $k_N/a_r$  is  $O(10^{-2})$  or smaller and  $\Phi'$  is in the range of 0.2 to 0.4 (see dotted line in Fig. 1).

The behavior of  $\mathbf{X}$  for the above range of  $k_p d$  and  $\Phi'$  is illustrated in Fig. 4. This figure shows that the dependency of  $\mathbf{X}$  on  $\Phi'$  is negligible, both with respect to an intercomparison of components of  $\mathbf{X}$ , and with respect to the dependency of  $X_d$  and  $X_T$  on the relative depth  $k_p d$ . For  $D$ ,  $\psi_c$  and  $H$ ,  $\mathbf{X}$  is independent of the relative depth. The (absolute) amplification factors are approximately 0.7, 1 and 1.7, respectively. The amplification factors for the depth  $d$  and the wave period  $T$  strongly depend on the relative depth  $k_p d$ . For large relative depths ( $k_p d > 2$ ), the relative variability of  $d$  and  $T$  is strongly amplified ( $|X_d| > 3$  and  $|X_T| > 4$ ). For extremely shallow water, however ( $kd > 1$ ), the spread of the Shields number is similar to that of the depth ( $|X_d| \approx 1$ ), whereas it is fairly insensitive to variability of the period  $T$  ( $|X_T| < 0.5$ ).

The central limit theorem predicts that the pdf of  $\psi_n$  can be described using a normal distribution,

$$p(\Psi) = \frac{1}{\sqrt{2\pi}} e^{-0.5 \Psi^2}, \quad \Psi = \frac{\psi_n - \psi_{n,m}}{\sigma_\psi} \quad (19)$$

for a wide range of pdf's of components of  $\mathbf{x}$ . This is easily confirmed with Monte Carlo experiments (figures not presented here). Given this (or any other) pdf of  $\psi_n$ , the representative source term  $S_{b,r} \equiv E(S_b)$  follows from Bayes' theorem as:

$$S_{b,r} = P_I E(S_b | \psi_n < 1.2) + P_{II} E(S_b | \psi_n \geq 1.2) \quad (20)$$



Fig. 4. Amplification factors for  $\Phi'$  ranging from

where  $P_I = P(\psi_n < \text{no-ripple and ripple expected values of coverage for the gr (19) can be found$

Substituting (1) (see Appendix A)

$$\frac{k_{N,r}}{a_r} = P_I \frac{k_{N,0}}{a_r} +$$

$$\psi_{n,II} = \psi_n + p$$

The subscripts m a (that is, no realization roughness results in (1).

$$S_{b,r} = f_{w,r} \mu_r \frac{\tau}{2g}$$

Eqs. (21)–(23), (1 complicated part of number (Eqs. 13– because the statistic

(15)

(16)

(17)

(18)

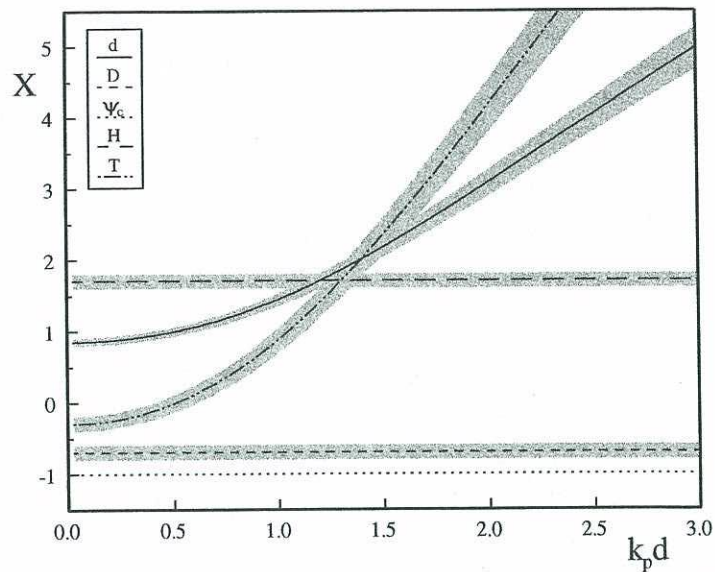


Fig. 4. Amplification factors  $X$  of Eqs. (15) as a function of the relative depth  $k_p d$ . Lines for  $\Phi' = 0.3$ , shaded areas for  $\Phi'$  ranging from 0.2 to 0.4.

in Eq. (5).

between the relative variance of components and the normalized Shields number ( $\sigma_\psi/\psi_{n,m}$ ). This corresponds to a decrease of  $\psi_n$ .

As  $k_p d$  and the normalized derivative of  $\psi_n$  are generally considered depth-limited, they are related as indicated from Fig. 1. For sediment motion with  $k_N = D \approx 0(1 \text{ mm})$  or smaller,  $k_N/a_r$  is 0.4 (see dotted line in Fig. 1).

The amplification factor  $X$  is illustrated in Fig. 4. This figure shows both  $X_d$  and  $X_T$  on the relative depth  $k_p d$ . The amplification factors for the relative depth  $k_p d$ . For large relative depth  $k_p d$ ,  $X_T$  is strongly amplified ( $|X_d| > 3$  and  $d > 1$ ), the spread of the Shields number is fairly insensitive to variability of the

of  $\psi_n$  can be described using a normal

(19)

This is easily confirmed with Monte Carlo simulation (or any other) pdf of  $\psi_n$ , the representative theorem as:

(20)

where  $P_I = P(\psi_n < 1.2)$  and  $P_{II} = P(\psi_n \leq 1.2)$  represent the probability of occurrence of the no-ripple and ripple regimes, respectively.  $E(\dots)$  represent the corresponding (conditional) expected values of  $S_b$ . Note that within this model  $P_{II}$  is by definition a fractional ripple coverage for the grid box considered. Explicit approximations for  $P_{I,II}$  corresponding to (19) can be found in, for instance, Abramowitz and Stegun (1973, pp. 923-933).

Substituting (1) in (20) and subsequent linearization and elimination of small terms (see Appendix A) results in the following subgrid roughness

$$\frac{k_{N,r}}{a_r} = P_I \frac{k_{IN,0}}{a_r} + P_{II} \left[ 1.5 \psi_{n,II}^{-2.5} + 0.0655 \left( \frac{u_r^2}{(s-1)ga_r} \right)^{1.4} \right] \quad (21)$$

$$\psi_{n,II} = \psi_n + p \left( \frac{1.2 - \psi_n}{\sigma_\psi} \right) \frac{\sigma_\psi}{P_{II}} \quad (22)$$

The subscripts m are dropped as these equations contain averaged parameter values only (that is, no realizations of stochastic parameters). Substituted in Eqs. (2) and (3), this roughness results in a representative friction factor  $f_{w,r}$  and a source term equivalent to Eq. (1).

$$S_{b,r} = f_{w,r} u_r \frac{\omega^2}{2g \sinh^2 kd} F \quad (23)$$

Eqs. (21)-(23), (13)-(19) and (2)-(4) result in a fairly simple subgrid model. The most complicated part of this model is the calculation of the spread of the normalized Shields number (Eqs. 13-18). This part of the model could be simplified further, particularly because the statistical data required to evaluate these equations are generally not available.

The simplest approach possible defines a single universal relative spread of the normalized Shields number. This, however, ignores the potentially strong dependency of  $\sigma_\psi/\psi_n$  on  $k_p d$ , which is related to the relative spread of the depth and the wave period (Fig. 4). The spread of the depth is generally expected to dominate the spread of the wave period because (i) the differences of the depth between neighbouring grid points around shoals (see, for instance, Fig. 3a) implies a significant subgrid variability of the depth, and (ii) wave periods generally vary slowly in space and time (for swell without currents, the variability of  $T$  is generally negligible). The spread of the depth can be divided into two parts. The first is the spread in depth related to the large-scale depth variations resolved by the grid ( $\sigma_{d,g}$ ). This variability can be estimated from the difference in depth between the grid point considered and adjacent grid points. The second component of the spread of the depth  $d$  is some universal subgrid spread  $\sigma_{d,s}$ . Finally combining the relative spread of  $D$ ,  $\psi_c$  and  $H$  in a single relative spread  $\sigma_{0,r}$ , the following simplified expression is found

$$\frac{\sigma_\psi}{\psi_n} \approx \left[ \sigma_{0,r}^2 + X_d^2 \left( \frac{\sigma_{d,g} + \sigma_{d,s}}{d} \right)^2 \right]^{1/2} \quad (24)$$

Obviously,  $X_d$  can be replaced by other (similar) functions of  $k_p d$  without loss of generality. The necessity of accurate estimates of  $\sigma_\psi/\psi_n$  will be discussed in the following sections, where several simplified expressions for  $\sigma_\psi/\psi_n$  will be used.

#### 4. Applications

The subgrid moveable-bed roughness model defined by Eqs. (21)–(23), (2)–(4), (19) and estimates for  $\sigma_\psi/\psi_n$  and  $P_{1,II}$  is applied to the swell propagation case of Fig. 3 and to an idealized case of depth-limited wave growth. Calculations have been performed with third-generation wave model WAVEWATCH (Tolman, 1991, 1992), in which this source term has been introduced. The appropriate (reduced) equations of WAVEWATCH will be presented below. This model features an integration method for source terms with dynamically adjusted time steps and a second order accurate propagation scheme. To simulate a typical shelf sea model, the grid and time increments are chosen as  $\Delta x = 25$  km and  $\Delta t = 15$  min. Note that wave models like WAVEWATCH by definition consider the evolution of the wave field in time. Steady solutions have been obtained by continuing the calculation over a sufficiently long time, keeping boundary conditions constant where necessary.

##### 4.1. Swell propagation

The first application of the present model considers the idealized swell propagation case of Fig. 3. In such conditions the governing equation of WAVEWATCH reduces to

$$\frac{\partial F(f, \theta)}{\partial t} + \frac{\partial c_g F(f, \theta)}{\partial x} = S_{b,r}(f, \theta) \quad (25)$$

and swell is simulated by considering energy in a single discrete component of the spectrum only. Excellent results are obtained with the correct sediment data ( $D = 0.2$  mm,  $\psi_c = 0.05$

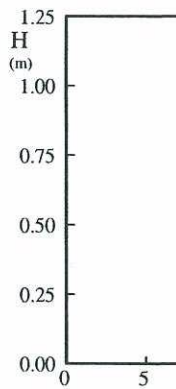


Fig. 5. Evolution in time of subgrid model (solid line,

and  $k_{N,0} = 0.01$  m) at 3). The latter implies the irregular bottom. ranges from 0.05 to  $\sigma_\psi/\psi_n \equiv 0.05$  (○ in overestimated ( $\sigma_\psi/\psi_n$  estimated in the no-ripple corresponding decay of the attenuation rate sediment parameters. 3), the transmitted wave ripple formation is not swell height become

Note that for the case of steady solution. If E contains systematic noise smooth beds and steep

##### 4.2. Depth-limited wave

In this section the wave growth, to assess in particular for coral reef estimated for quasi-steady WAVEWATCH reduces to:

$$\frac{\partial F(f, \theta)}{\partial t} = S_m(f, \theta)$$

The source terms other than (Tolman, 1988; for cycle 4 see



iversal relative spread of the normalized  
lly strong dependency of  $\sigma_\psi/\psi_n$  on  $k_p d$ ,  
nd the wave period (Fig. 4). The spread  
spread of the wave period because (i)  
ig grid points around shoals (see, for  
riability of the depth, and (ii) wave  
or swell without currents, the variability  
pth can be divided into two parts. The  
e depth variations resolved by the grid  
fference in depth between the grid point  
mponent of the spread of the depth  $d$  is  
ing the relative spread of  $D$ ,  $\psi_c$  and  $H$  in  
d expression is found

$$(24)$$

ctions of  $k_p d$  without loss of generality.  
be discussed in the following sections,  
l be used.

ned by Eqs. (21)–(23), (2)–(4), (19)  
swell propagation case of Fig. 3 and to  
calculations have been performed with  
an, 1991, 1992), in which this source  
ed) equations of WAVEWATCH will be  
method for source terms with dynam-  
ate propagation scheme. To simulate a  
s are chosen as  $\Delta x = 25$  km and  $\Delta t = 15$   
definition consider the evolution of the  
ined by continuing the calculation over  
ns constant where necessary.

rs the idealized swell propagation case  
of WAVEWATCH reduces to

$$(25)$$

gle discrete component of the spectrum  
sediment data ( $D = 0.2$  mm,  $\psi_c = 0.05$

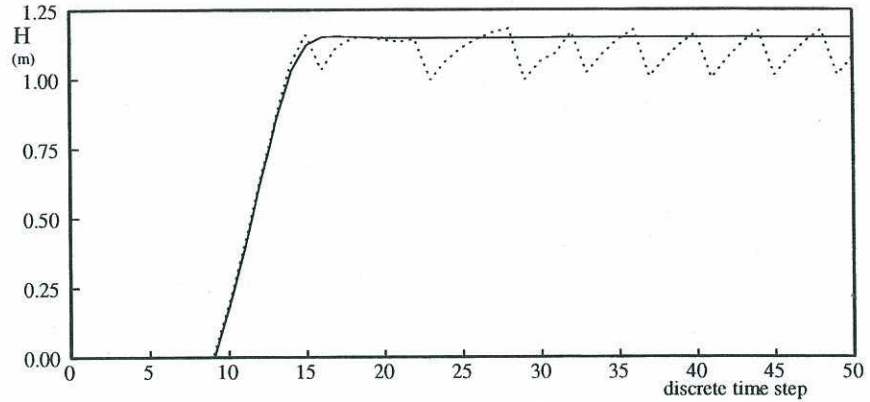


Fig. 5. Evolution in time of the wave height at point A in Fig. 3 for the discontinuous model (dotted line) and the subgrid model (solid line, corresponding to ● in Fig. 3).

and  $k_{N,0} = 0.01$  m) and the best possible estimate of  $\sigma_\psi/\psi_n$  based on Eq. (24) (● in Fig. 3). The latter implies that  $\sigma_{0,r} = 0.07$  and that  $(\sigma_{d,g} + \sigma_{d,s})/d$  is calculated directly from the irregular bottom. The corresponding normalized spread of the Shields number  $\sigma_\psi/\psi_n$  ranges from 0.05 to 0.15. Similarly good results are obtained for a small constant spread  $\sigma_\psi/\psi_n \equiv 0.05$  (○ in Fig. 3). Small errors are introduced if the spread is systematically overestimated ( $\sigma_\psi/\psi_n \equiv 0.30$ , △ in Fig. 3). The friction factor then is systematically overestimated in the no-ripple regime (△ in Fig. 3b) resulting in a slight overestimation of the corresponding decay rate of the wave height (△ in Fig. 3a), and the discontinuous behavior of the attenuation rate is obscured. The model, however, is more sensitive to its mean sediment parameters. If the grain diameter is overestimated by 50% ( $D = 0.3$  mm, □ in Fig. 3), the transmitted wave height over and beyond the shoal is significantly overestimated. If ripple formation is neglected altogether ( $k_N \equiv k_{N,0}$ , \* in Fig. 3) errors in the transmitted swell height become even larger.

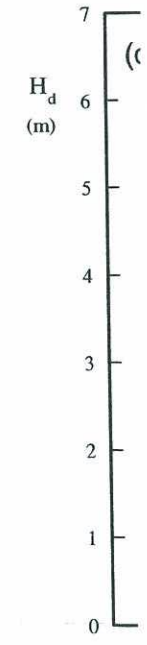
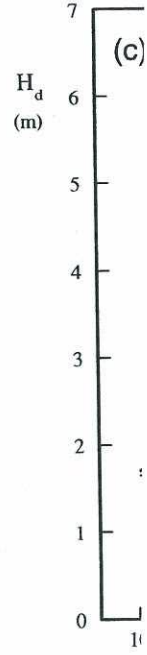
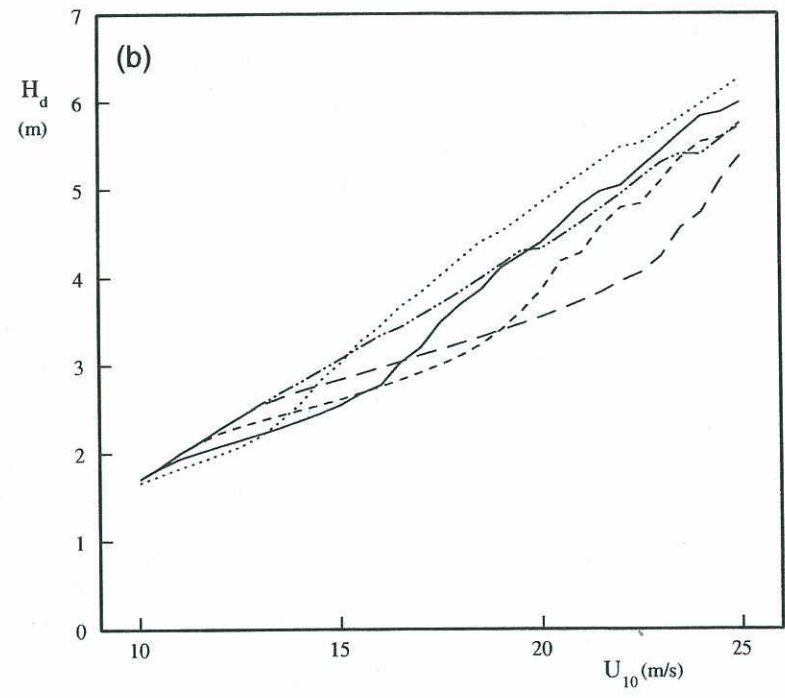
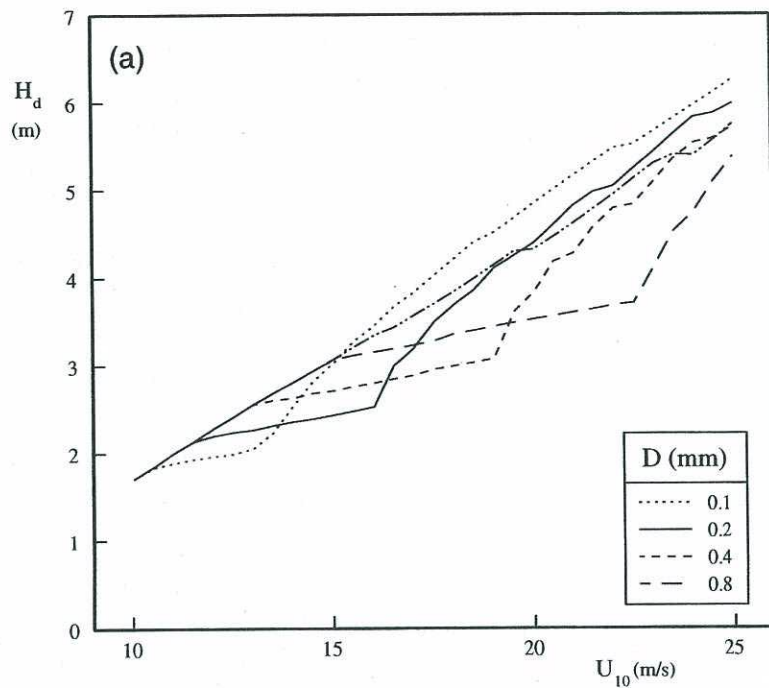
Note that for the case considered here, a subgrid approach proved necessary to obtain a steady solution. If Eqs. (1)–(6) are used directly, the “steady” solution on the shoal contains systematic modulations of  $H$  of up to 20% due to roughnesses alternating between smooth beds and steep ripples (dotted line in Fig. 5).

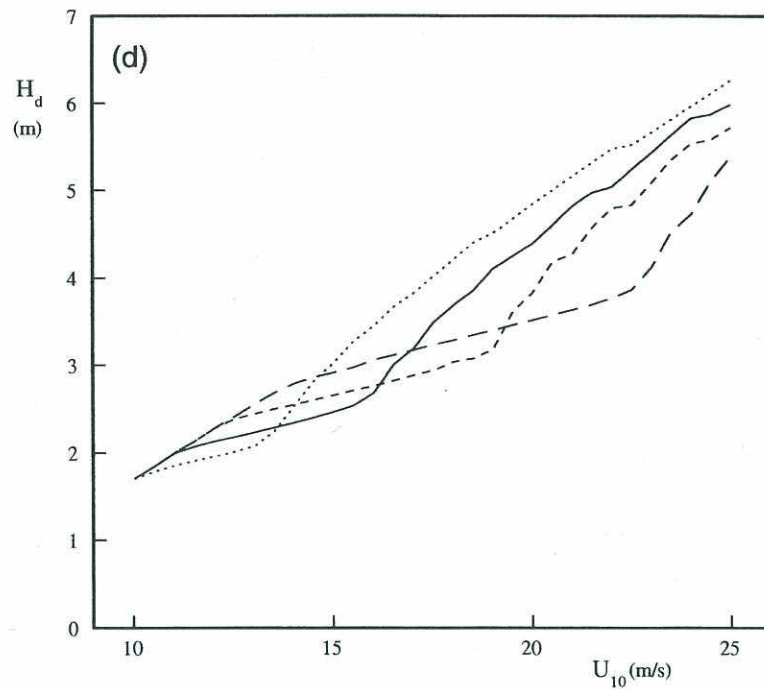
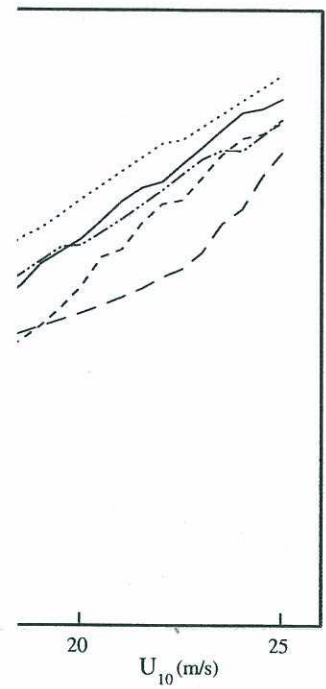
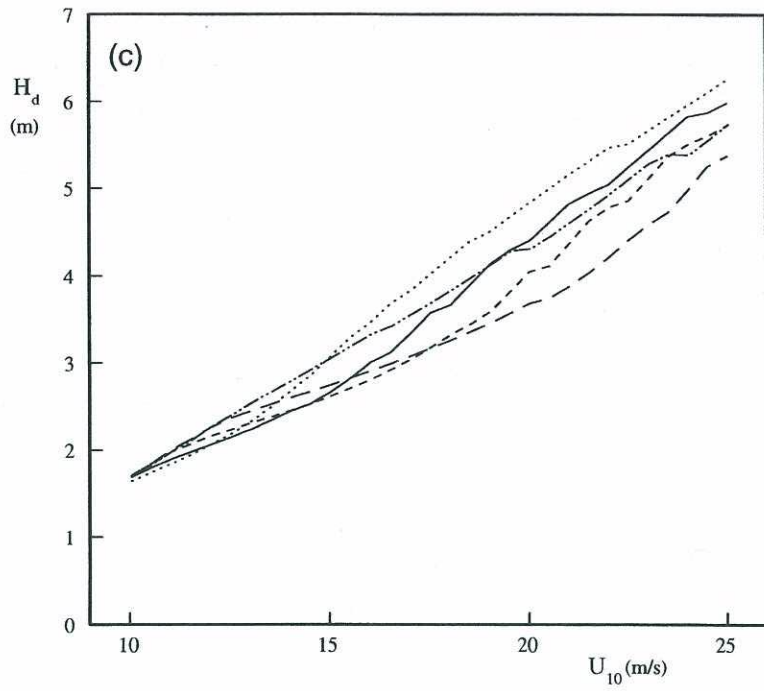
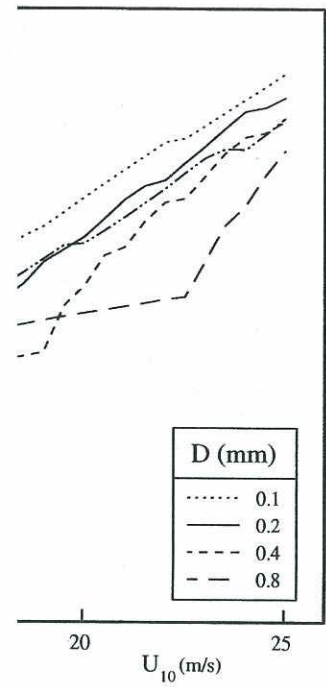
#### 4.2. Depth-limited wind seas

In this section the subgrid moveable-bed roughness model is applied to depth-limited wave growth, to assess the sensitivity of depth-limited wave heights to sediment conditions, in particular for conditions of initial ripple formation. Depth-limited wave heights are estimated for quasi-homogeneous conditions, for which the governing equation of WAVEWATCH reduces to:

$$\frac{\partial F(f, \theta)}{\partial t} = S_{in}(f, \theta) + S_{nl}(f, \theta) + S_{ds}(f, \theta) + S_{b,r}(f, \theta) \quad (26)$$

The source terms other than  $S_{b,r}$  are identical to those of cycle 4 of the WAM model (WAMDIG, 1988; for cycle 4 see, e.g. Mastenbroek et al., 1993). Wind input and dissipation ( $S_{in}$  and





roughness model. This has two implications. First, it is confirmed that moveable-bed effects are generally not important for the modeling of depth-limited wind seas. Secondly, a subgrid approach is needed to avoid unrealistic sensitivities of depth-limited wind seas to sediment parameters if a moveable-bed model is implemented (for instance to accurately describe swell attenuation). The large spread of the normalized Shields number as occurs for large relative depths are essential to remove the above unrealistic behavior.

The present subgrid model has two potential shortcomings. First, the discontinuous roughness model (6) on which the subgrid model is based is not yet satisfactorily validated and is open for improvements (see Tolman, 1994). Secondly, the local applicability of the discontinuous model can be questioned.

The discontinuous roughness model (6) is based on limited laboratory data, and does not include any data in which a mean current is present. Although from a hydrodynamic point of view wave-current interactions are not expected to influence the bottom friction source term significantly (see Tolman, 1994, page 1006), currents can be expected to modify bed forms, and hence influence the roughnesses. In particular in near-shore areas, where currents can be strong, the applicability of the present model therefore is potentially limited. In general, more data is necessary to validate this and other roughness model. In particular field observations and observations including waves and currents would be useful.

The best documented part of the roughness model (6) is its discontinuous behavior as a function of the Shields number (Tolman, 1994). This discontinuous behavior in turn results in the need for a subgrid approach. New parameterizations of moveable-bed roughnesses in different wave-sediment interaction regimes can easily be implemented in Eq. (21). Thus, additional observations might significantly change behavior of moveable-bed roughness models, but are not expected to have an impact on the present subgrid approach, as long as the roughness parameterizations can be expressed in terms of a Shields number.

The present subgrid model assumes the local applicability of the roughness model Eq. (6). This results in extreme changes of the roughness on small scales (Fig. 3b), suggesting the present statistical approach. Such behavior is in qualitative agreement with the observation of small ripple patches in nature (e.g., Cacchione and Drake, 1982), but it is not in agreement with the observations of a transition regime of undeveloped ripples for near-critical Shields numbers as reported by Amos et al. (1988). Amos et al. attribute this transition to a balance between ripple formation by waves and ripple degradation due to bioturbation. This suggests a different approach to modeling a continuous transition between the ripple and no-ripple regimes, using a local ripple evolution model instead of spatial statistics.

A ripple evolution model requires parameterizations for ripple evolution in time. To the knowledge of the present author, data required for such parameterizations is insufficient and qualitative at best (e.g., Brebner, 1980; Amos et al., 1988; Drake and Cacchione, 1989; Green et al., 1990). Such a model could furthermore include statistical information of the local wave field, to estimate the fraction of individual waves which move sediment and hence contribute to ripple formation. Without derivation of an actual model, it appears evident that such a model could be expressed in a form similar to Eq. (21), where  $P_{II}$  represents fractional ripple development instead of a fractional ripple coverage (as in the present model). From a wave modeling perspective both approaches are identical, as long as they result in the same representative roughness.

Finally, an alternative to qualitatively explain the undeveloped ripples.  $0.05 < P_{II} < 0.95$  and as this transition regime encompasses this results in the ratio of the zone as observed by Amos et al.

## 6. Conclusions

A statistical subgrid model in large-scale wind wave roughness on subgrid scales in conditions of initial ripple depth-limited wind seas strong dependency of model regimes. The present subgrid bed roughness models. transition regime with t

## Acknowledgements

The author thanks F. Paul E. Long Jr. and D.

## Appendix A. Derivation

Substitution of the c (20) yields

$$S_{b,r} = -\frac{1}{2g} \sum_{\beta} P_{\beta} f$$

where  $\beta = I, II$  denotes subgrid model remains equation becomes

$$S_{b,r} = -\frac{\omega^2}{2g \sinh^2 k}$$

This equation requires an arbitrary parameter

irmed that moveable-bed effects d wind seas. Secondly, a subgrid h-limited wind seas to sediment instance to accurately describe elds number as occurs for large c behavior.

mings. First, the discontinuous is not yet satisfactorily validated lly, the local applicability of the

imited laboratory data, and does Although from a hydrodynamic to influence the bottom friction ), currents can be expected to n particular in near-shore areas, t model therefore is potentially and other roughness model. In /es and currents would be useful. s its discontinuous behavior as a ntinuous behavior in turn results s of moveable-bed roughnesses y be implemented in Eq. (21). ehavior of moveable-bed rough- he present subgrid approach, as n terms of a Shields number.

ility of the roughness model Eq. all scales (Fig. 3b), suggesting ative agreement with the obser- and Drake, 1982), but it is not in f undeveloped ripples for near- 88). Amos et al. attribute this s and ripple degradation due to ; a continuous transition between lution model instead of spatial

ripple evolution in time. To the parameterizations is insufficient 88; Drake and Cacchione, 1989; ide statistical information of the aves which move sediment and of an actual model, it appears similar to Eq. (21), where  $P_{II}$  ional ripple coverage (as in the approaches are identical, as long

Finally, an alternative interpretation of  $P_{II}$  as a fractional ripple development can be used to qualitatively explain the range of Shields numbers for which Amos et al. (1988) observed undeveloped ripples. Assuming (arbitrarily) that undeveloped ripples correspond to  $0.05 < P_{II} < 0.95$  and assuming a normal distribution for  $\psi_n$  within the spectrum, the transition regime encompasses a range of mean Shields numbers  $\Delta\psi_n = 3.3\sigma_{\psi}$ . For  $\sigma_{\psi}/\psi_n = 0.2$ , this results in the ratio of 2 between the highest and lowest Shields number of the transition zone as observed by Amos et al. (1988).

## 6. Conclusions

A statistical subgrid moveable-bed bottom friction model is developed for the application in large-scale wind wave models. This model accounts for the spatial variability of bottom roughness on subgrid scales. It reproduces the discontinuous attenuation behavior of swell in conditions of initial ripple formation, as predicted by the "exact" model. Application to depth-limited wind seas indicates that a subgrid model is required to avoid an unrealistically strong dependency of mildly depth-limited wind seas on sediment conditions and roughness regimes. The present subgrid approach is easily applied to other (discontinuous) moveable-bed roughness models. An alternative interpretation of the subgrid model can explain the transition regime with undeveloped ripples as observed by Amos et al. (1988).

## Acknowledgements

The author thanks Peter Janssen for supplying computer code of his source terms to facilitate implementation in WAVEWATCH, and Dean G. Duffy, Dmitry Chalikov, W. Perrie, Paul E. Long Jr. and D.B. Rao for discussing drafts of this paper.

## Appendix A. Derivation of the subgrid model

Substitution of the discontinuous source term (1) in the general subgrid source term (20) yields

$$S_{b,r} = -\frac{1}{2g} \sum_{\beta} P_{\beta} f_{w,\beta} u_{r,\beta} \frac{\omega^2}{\sinh^2 kd} F \quad (A1)$$

where  $\beta = I, II$  denotes the two ripple regimes as in Eqs. (20) and (21). Assuming that the subgrid model remains quasi-linear with respect to the near-bottom velocity spectrum, this equation becomes

$$S_{b,r} = -\frac{\omega^2}{2g \sinh^2 kd} F \sum_{\beta} P_{\beta} f_{w,\beta} u_{r,\beta} \quad (A2)$$

This equation requires estimates of mean parameter values in both roughness regimes. For an arbitrary parameter  $y(x)$ , linearization gives the following estimate of  $y_{\beta}$ .

$$y_{\beta} = y_m + \frac{\text{Cov}(y, \psi_n)}{\sigma_{\psi}^2} (\psi_{n,\beta} - \psi_{n,m}) \quad (\text{A3})$$

$$\frac{\text{Cov}(y, \psi_n)}{y_m \psi_{n,m}} = \sum_{i=1}^5 X_i Y_i \left( \frac{\sigma_i}{x_{i,m}} \right)^2 \quad (\text{A4})$$

$$Y_i = \frac{x_{i,m}}{y_m} \frac{\partial y}{\partial x_i} \quad (\text{A5})$$

The mean normalized Shields numbers for both roughness regimes are calculated as (using Abramowitz and Stegun, 1973, section 26.2.45)

$$\psi_{n,\beta} = \psi_{n,m} \mp p \left( \frac{1.2 - \psi_n}{\sigma_{\psi}} \right) \frac{\sigma_{\psi}}{P_{\beta}} \quad (\text{A6})$$

where the minus is used in the no-ripple regime ( $\beta=1$ ) and where  $p(\dots)$  is the standard normal pdf (19). However, the corrections  $y_{\beta} - y_m$  for  $u_r$  and  $a_r$  as given by Eq. (A3) are generally small and their effects partially cancel. Thus Eq. (A2) can be approximated as

$$S_{b,r} = -u_{r,m} \frac{\omega^2}{2g \sinh^2 kd} F \sum_{\beta} P_{\beta} f_{w,\beta} \quad (\text{A7})$$

Numerical experiments furthermore show that the representative friction factor  $\sum_{\beta} P_{\beta} f_{w,\beta}$  can be replaced by a single representative friction factor  $f_{w,r}$  calculated from the representative roughness given by Eqs. (21) and (22). Note that Eq. (22) still incorporates an estimate of  $\psi_n$  specific for the ripple regime. The correction of the normalized Shields number for the ripple regime (right term in Eq. 22) has been maintained to ensure that the corresponding part of the representative roughness remains within its range of validity. Replacing  $\psi_{n,II}$  by  $\psi_{n,m}$  has a much bigger impact than the above simplifications, and can lead to differences of  $O(10\%)$  in the source term.

## References

- Abramowitz, M. and Stegun, I.A., 1973. Handbook of Mathematical Functions, 9th print. Dover Publications, New York, 1046 pp.
- Amos, C.L., Bowen, A.J., Huntley, D.A. and Lewis, C.F.M., 1988. Ripple generation under combined influence of waves and currents on the Canadian continental shelf. Cont. Shelf Res., 8: 1129-1153.
- Brebner, A., 1980. Sand bed-form lengths under oscillatory motion. In: Proc. 17th Int. Conf. Coastal Eng., Sidney. ASCE, pp. 1340-1343.
- Cacchione, D.A. and Drake, D.E., 1982. Measurements of storm generated bottom stresses on the continental shelf. J. Geophys. Res., 87: 1952-1961.
- Cacchione, D.A., Grant, W.D., Drake, D.E. and Glenn, S.M., 1987. Storm-dominated bottom boundary layer dynamics on the northern California continental shelf: Measurements and predictions. J. Geophys. Res., 92: 1817-1827.
- Drake, D.E. and Cacchione, D.A., 1986. Field observations of bed shear stress and sediment resuspension on shelves. Cont. Shelf Res., 6: 415-429.
- Drake, D.E. and Cacchione, D.A., 1989. Estimates of the suspended sediment concentration ( $C_s$ ) and resuspension coefficient ( $\gamma_0$ ) from near-bottom observations on the California shelf. Cont. Shelf Res., 9: 51-64.

- Glenn, S.M. and Grant, W.D., 1987. Storm-dominated bottom boundary layer dynamics on the northern California shelf. J. Geophys. Res., 92: 1817-1827.
- Grabner, H.C. and Madsen, O., 1988. Storm-dominated bottom boundary layer dynamics on the northern California shelf. J. Geophys. Res., 93: 469-481.
- Green, M.O., Rees, J.M. and Madsen, O., 1989. Storm-dominated bottom boundary layer dynamics on the northern California shelf. J. Geophys. Res., 94: 1817-1827.
- Gross, T.F., Isley, A.E. and Madsen, O., 1989. Storm-dominated bottom boundary layer dynamics on the northern California shelf. J. Geophys. Res., 94: 1817-1827.
- Hasselmann, S. and Hasselmann, K., 1987. Storm-dominated bottom boundary layer dynamics on the northern California shelf. J. Geophys. Res., 92: 1817-1827.
- Janssen, P.A.E.M., 1989. Wind waves on the sea. J. Geophys. Res., 94: 745-754.
- Janssen, P.A.E.M., 1991. Quasi-steady state wind waves on the sea. Oceanogr., 21: 1631-1644.
- Madsen, O.S. and Grant, W.D., 1987. Storm-dominated bottom boundary layer dynamics on the northern California shelf. Honolulua Conf. Coastal Eng., Honolulu.
- Madsen, O.S. and Rosengaus, J., 1987. Storm-dominated bottom boundary layer dynamics on the northern California shelf. 21st Int. Conf. Coastal Eng., Honolulu.
- Madsen, O.S., Poon, Y.-K. and Grant, W.D., 1987. Storm-dominated bottom boundary layer dynamics on the northern California shelf. 21st Int. Conf. Coastal Eng., Honolulu.
- Madsen, O.S., Mathiesen, P.I. and Grant, W.D., 1987. Storm-dominated bottom boundary layer dynamics on the northern California shelf. Proc. 22nd Int. Conf. Coastal Eng., Honolulu.
- Masterbroek, C., Burgers, G. and Madsen, O.S., 1987. Storm-dominated bottom boundary layer dynamics on the northern California shelf. Proc. 22nd Int. Conf. Coastal Eng., Honolulu.
- Shemdin, O., Hasselmann, K. and Madsen, O.S., 1987. Storm-dominated bottom boundary layer dynamics on the northern California shelf. In: Turteltaub, P. (ed.) Ser. V, Vol. 1, pp. 347-358. SWIM Group, 1985. A shallow water model. R. Meteor. Soc., 111: 1087-1100.
- Tolman, H.L., 1991. A third-order shallow water model. J. Phys. Oceanogr., 21: 1087-1100.
- Tolman, H.L., 1992. Effects of wind waves on the sea. J. Geophys. Res., 97: 1095-1111.
- Tolman, H.L., 1994. Wind waves on the sea. WAMDIAG, 1988: The WAM model. J. Geophys. Res., 93: 1775-1810.
- Weber, S.L., 1991. Eddy-viscosity and sediment resuspension. J. Geophys. Res., 96: 73-98.
- Wilson, K.C., 1989. Friction factor for wind waves on the sea. J. Geophys. Res., 94: 1817-1827.

(A3)

(A4)

(A5)

(A6)

(A7)

Glenn, S.M. and Grant, W.D., 1987. A suspended sediment stratification correction for combined wave and current flows. *J. Geophys. Res.*, 92: 8244-8264.

Graber, H.C. and Madsen, O.S., 1988. A finite-depth wind-wave model. Part I: Model description. *J. Phys. Oceanogr.*, 18: 1465-1483.

Grant, W.D. and Madsen, O.S., 1982. Movable bed roughness in unsteady oscillatory flow. *J. Geophys. Res.*, 87: 469-481.

Green, M.O., Rees, J.M. and Pearson, N.D., 1990. Evidence for the influence of wave-current interaction in a tidal boundary layer. *J. Geophys. Res.*, 95: 9629-9644.

Gross, T.F., Isley, A.E. and Sherwood, C.R., 1992. Estimation of stress and bed roughness during storms on the northern California shelf. *Cont. Shelf Res.*, 12: 389-413.

Hasselmann, S. and Hasselmann, K., 1985. Computations and parameterizations of the nonlinear energy transfer in a gravity-wave spectrum. Part II: Parameterizations of the nonlinear energy transfer for application in wave models. *J. Phys. Oceanogr.*, 15: 1378-1391.

Janssen, P.A.E.M., 1989. Wave induced stress and the drag of air flow over sea waves. *J. Phys. Oceanogr.*, 19: 745-754.

Janssen, P.A.E.M., 1991. Quasi-linear theory of wind-wave generation applied to wave forecasting. *J. Phys. Oceanogr.*, 21: 1631-1642.

Madsen, O.S. and Grant, W.D., 1976. Quantitative description of sediment transport by waves. In: *Proc. 15th Int. Conf. Coastal Eng.*, Honolulu, HI. ASCE, pp. 1093-1112.

Madsen, O.S. and Rosengaus, M.M., 1988. Spectral wave attenuation by bottom friction: experiments. In: *Proc. 21st Int. Conf. Coastal Eng.*, Malaga. ASCE, pp. 849-857.

Madsen, O.S., Poon, Y.-K. and Graber, H.C., 1988. Spectral wave attenuation by bottom friction: theory. In: *Proc. 21st Int. Conf. Coastal Eng.*, Malaga. ASCE, pp. 492-504.

Madsen, O.S., Mathiesen, P.P. and Rosengaus, M.M., 1990. Movable bed friction factors for spectral waves. In: *Proc. 22nd Int. Conf. Coastal Eng.*, Delft. ASCE, pp. 420-429.

Mastenbroek, C., Burgers, G. and Janssen, P.A.E.M., 1993. The dynamic coupling of a wave model and a storm surge model through the atmospheric boundary layer. *J. Phys. Oceanogr.*, 23: 1856-1866.

Shemdin, O., Hasselmann, K., Hsiao, S.V. and Heterich, K., 1978. Nonlinear and linear bottom interaction effects in shallow water. In: *Turbulent Fluxes through the Sea Surface, Wave Dynamics and Prediction*. NATO Conf. Ser. V, Vol. 1, pp. 347-365.

SWIM Group, 1985. A shallow water intercomparison of three numerical wave prediction models (SWIM). *Q. J. R. Meteor. Soc.*, 111: 1087-1112.

Tolman, H.L., 1991. A third-generation model for wind waves on slowly varying, unsteady and inhomogeneous depths and currents. *J. Phys. Oceanogr.*, 21: 782-797.

Tolman, H.L., 1992. Effects of numerics on the physics in a third-generation wind-wave model. *J. Phys. Oceanogr.*, 22: 1095-1111.

Tolman, H.L., 1994. Wind waves and moveable-bed bottom friction. *J. Phys. Oceanogr.*, 24: 994-1009.

WAMDIG, 1988. The WAM model — a third generation ocean wave prediction model. *J. Phys. Oceanogr.*, 18: 1775-1810.

Weber, S.L., 1991. Eddy-viscosity and drag-law models for random ocean wave dissipation. *J. Fluid Mech.*, 232: 73-98.

Wilson, K.C., 1989. Friction on wave induced sheet flow. *Coastal Eng.*, 13: 371-379.

roughness regimes are calculated as (using

$\beta=1$ ) and where  $p(\dots)$  is the standard deviation for  $u_r$  and  $a_r$  as given by Eq. (A3) are used. Eq. (A2) can be approximated as

representative friction factor  $\sum_{\beta} P_{\beta} f_{w,\beta}$  factor  $f_{w,r}$  calculated from the representative that Eq. (22) still incorporates an correction of the normalized Shields has been maintained to ensure that the remains within its range of validity. than the above simplifications, and can

Mathematical Functions, 9th print. Dover Publications,

1988. Ripple generation under combined influence of wind and current. *Cont. Shelf Res.*, 8: 1129-1153.

on. In: *Proc. 17th Int. Conf. Coastal Eng.*, Sidney.

bottom generated bottom stresses on the continental

1987. Storm-dominated bottom boundary layer measurements and predictions. *J. Geophys. Res.*, 92:

bed shear stress and sediment resuspension on

offshore sediment concentration ( $C_a$ ) and resuspension on the northern California shelf. *Cont. Shelf Res.*, 9: 51-64.